PLOS ONE

RESEARCH ARTICLE

# GIS-based flood hazard mapping using relative frequency ratio method: A case study of Panjkora River Basin, eastern Hindu Kush, Pakistan

**Kashif Ullah**[1], **Jiquan Zhang**[1,2,3]*

**1** Institute of Natural Disaster Research, School of Environment, Northeast Normal University, Changchun, China, **2** State Environmental Protection Key Laboratory of Wetland Ecology and Vegetation Restoration, Northeast Normal University, Changchun, China, **3** Key Laboratory for Vegetation Ecology, Ministry of Education, Changchun, China

* zhangjq022@nenu.edu.cn





**Citation:** Ullah K, Zhang J (2020) GIS-based flood hazard mapping using relative frequency ratio method: A case study of Panjkora River Basin, eastern Hindu Kush, Pakistan. PLoS ONE 15(3): e0229153. https://doi.org/10.1371/journal.pone.0229153

**Editor:** Mou Leong Tan, Universiti Sains Malaysia, MALAYSIA

**Received:** October 21, 2019

**Accepted:** January 30, 2020

**Published:** March 25, 2020



**Data Availability Statement:** All relevant data are within the manuscript and attached in Supporting Information files. Landsat-8(OLI) imagery (Date: 19-September-2018) and ASTER DEM can downloaded from USGS official website (https://earthexplorer.usgs.gov).

**Funding:** This research is supported by the national key research and development program of china (2018YFC1508804); The Key Scientific and Technology Research and Development Program of Jilin Province (20180201033SF); The Key

## Abstract

Flood is the most devastating and prevalent disaster among all-natural disasters. Every year, flood claims hundreds of human lives and causes damage to the worldwide economy and environment. Consequently, the identification of flood-vulnerable areas is important for comprehensive flood risk management. The main objective of this study is to delineate flood-prone areas in the Panjkora River Basin (PRB), eastern Hindu Kush, Pakistan. An initial extensive field survey and interpretation of Landsat-7 and Google Earth images identified 154 flood locations that were inundated in 2010 floods. Of the total, 70% of flood locations were randomly used for building a model and 30% were used for validation of the model. Eight flood parameters including slope, elevation, land use, Normalized Difference Vegetation Index (NDVI), topographic wetness index (TWI), drainage density, and rainfall were used to map the flood-prone areas in the study region. The relative frequency ratio was used to determine the correlation between each class of flood parameter and flood occurrences. All of the factors were resampled into a pixel size of 30×30 m and were reclassified through the natural break method. Finally, a final hazard map was prepared and reclassified into five classes, i.e., very low, low, moderate, high, very high susceptibility. The results of the model were found reliable with area under curve values for success and prediction rate of 82.04% and 84.74%, respectively. The findings of this study can play a key role in flood hazard management in the target region; they can be used by the local disaster management authority, researchers, planners, local government, and line agencies dealing with flood risk management.

## 1. Introduction

Flood is the most prevalent and devastating natural disaster among all natural disasters that have adverse impacts on human health, natural and artificial environments [1,2]. Flood is a major risk to human life (loss of life, injury), assets (agriculture area, yield production, homes,

Scientific and Technology Research and Development Program of Jilin Province (20180201035SF); The Key Scientific and Technology Program of Jilin Province (20170204035SF). The funders provided support in the form of salaries for authors [Jiquan Zhang], but did not have any additional role in the study design, data collection and analysis, decision to publish, or preparation of the manuscript.

**Competing interests:** The authors have declared that no competing interests exist.

and buildings), communication systems (urban infrastructure, bridges, roads, and railway lines), culture heritage, and ecosystems [1–3]. Literature indicates that more than 2000 deaths occur every year due to flooding, and more than 75 million people are adversely affected in one way or another across the globe [2,3]. Many factors, including both natural and anthropogenic are responsible for catastrophic flood incidents. Flood occurs due to heavy rainfall or snow melt that overflows to adjacent areas, or flood plains, and temporarily inundates the surrounding areas [4,5]. Recent studies, indicating that climate change is a fundamental factor that induces flood in various parts of the world [6,7], Charlton et al. [8] indicate that flood disasters in a region can be considerably influenced by changes in land use patterns forming an impermeable surface, which may increase flow velocity. Aside from these, many other factors that trigger flood occurrence are: slope, elevation, land use, curvature, Normalized Difference Vegetation Index (NDVI), proximity to rivers, etc., [9,10]. Due to the complex nature of floods, their frequent occurrence and extensive destruction across the globe, a large number of scientists have devoted significant effort to investigate and understand flood hazard for better mitigation and management [4,11–14].

Flood is a natural phenomenon and its complete prevention is not possible; however, the risk of the flood can be minimized by appropriate planning and mitigation measures. Flood management is one of the key steps in mitigation and risk reduction. Various studies have indicated that identification of flood risk zones and application of essential risk reduction measures (structural and non-structural) can effectively reduce flood losses to an acceptable level [14,15]. Moreover, flood hazard mapping plays a significant role in flood planning, early warning systems, emergency response services, and design of flood risk reduction measures [14,16]. So far, various studies have been conducted to assess and map flood-prone areas in different regions of the world [9,17,18]. The study of Guo et al.[14] stated that the scope of conventional approaches for flood hazard mapping is usually narrow, due to a lack of sufficient data. For example, rainfall-runoff modeling methods, watermarks on buildings, models involving numerical simulations, etc., are not appropriate for comprehensive river and flood analysis [2,10]. The acquisition of adequate data for flood mapping using these methods and similar conventional techniques is expensive, time-consuming, and often not available at the watershed or regional level, especially in developing countries. Today, remote sensing and GIS are powerful tools and provide different data sources for hazard management, flood susceptibility, and its forecast [7,11,19].

Over the past few decades, numerous methods have been developed and used to investigate flood hazard and risk assessment. These methods include the analytical hierarchy process (AHP) [13,19], fuzzy logic and genetic algorithms [17], variable fuzzy theory [14], hydrological forecasting systems [20,21], random forest [22], artificial neural networks (ANNs) [18,22], adaptive neuro-fuzzy interface systems [23], logistic regression [24], weight of evidence [25,26], analytic network process (ANP) [27], statistical index [28], Shannon's entropy [29], Copula-Based Bayesian Network [30], and frequency ratio models [1,25,31]. The ANN approach, which has been used for flood susceptibility mapping [18,32], tries to make an association between some input factors and an outcome. However, Tiwari and Chaterjee [33] reported that the length of the dataset can cause errors in the process of ANN modelling and also poor prediction. Das [12] applied AHP to map flood hazard zonation in the Vaitarna basin, Maharashtra, India. However the drawback of AHP lies in its dependence on expert opinion [34]. The most common statistical methods of logistic regression and frequency ratio (FR) can be considered as significant methods that use a simple and understandable perception [1,25,26,35]. Tehrany et al. [9] reported that logistic regression and FR models can generate acceptable flood risk maps, and the process of analysis is easily understandable. Among bivariate statistical models, the FR model is considered one of the most important method that

is easy to apply and can produce acceptable risk analysis and mapping [9,26,35,36]. Accordingly, FR was selected from the set of bivariate statistical methods for this study. The results obtained from this model are easy to interpret. Although this model is infrequently used in flood hazard mapping, its superior performance has been proven in other fields of natural hazard such as landslides [34,37–40]. Furthermore, some studies show that bivariate statistical models sometimes have a higher accuracy than machine learning models, which require huge amounts of data as training for better accuracy [40–42]. FR is the bivariate statistical method that can consider the correlation between dependent factors (historical flood points) and independent factors (flood-causative factors) [1,25,43]. FR models have been successfully applied to flood susceptibility and vulnerability assessments in different flood prone regions of the world [1,25,26].

The Panjkora River Basin (PRB) is located in the eastern Hindu Kush region, Khyber Pakhtunkhwa province, Pakistan, which experiences flood events almost every year, generally during the monsoon seasons (June–September) [44]. Over the last decade, many disastrous floods have occurred in the region, which negatively affected human lives, property, agriculture, and other infrastructure [45–47]. The most devastating flood events have been recorded in the years 2005, 2010, 2014 and 2016. It has been reported by Rahman and Dawood [48] that climate change has intensified the spatiotemporal variability of rainfall, which poses serious threats to the local communities in the form of floods. In addition, the complex topography of the region coupled with the fragile socioeconomic condition of the local people triggers flood risk in the region [46]. So far, few studies have been conducted to assess flood hazards and map the flood-prone zones, especially in the middle and lower catchment of the PRB [46,47]. Therefore, the present study was designed to map the flood-prone areas in PRB and propose effective measures for flood risk reduction in the study region. The study is based on an integrated approach using ground-based observation, remote sensing, and relative frequency ratio (RFR) techniques. The current study is the first of its kind to map the flood-prone areas in the PRB using the RFR model.

## 2. Materials and methods

### 2.1 Description of the study area

The study area is located in the eastern Hindu Kush Khyber, Pakhtunkhwa province, Pakistan with the geographical extent of "34.33˚–35.0˚ N latitudes and 71.0˚–72.0˚ E longitudes" (Fig 1). It covers the lower and middle catchments of the PRB, and comprises an area of 1,741 $km^2$. A river runs through it northeast to southwest, joining up with tributaries and finally draining into the river Swat at Qalangi village [46]. Climatically, in winter, the temperature drops to -12 ˚C while in summer, the temperature rises to 35 ˚C. In monsoon seasons (June–September), the PRB receives more than 800 mm of rainfall [47]. In the study area, the soil structure varies from a clayey nature to loam and sandy loam. In most places, due to steep and delicate slopes, the ground is exposed and vulnerable to erosion. The fertile soils exist mostly on moderate slopes. Such areas are commonly used for agriculture.

In recent years, the study area experienced disastrous floods in 2005, 2010, 2014, and 2016 with adverse impacts on people lives, property, agriculture, and infrastructure [46,47]. During the summer season, heavy rainfall causes floods in the region, and sometimes the extraordinary activity of the monsoon causes high surface run-off and peak discharge.

### 2.2 Flood inventory mapping

The database of past floods is important to the study of the relationship between different flood triggering factors and flood occurrence [18,49]. Moreover, the accuracy of the flood

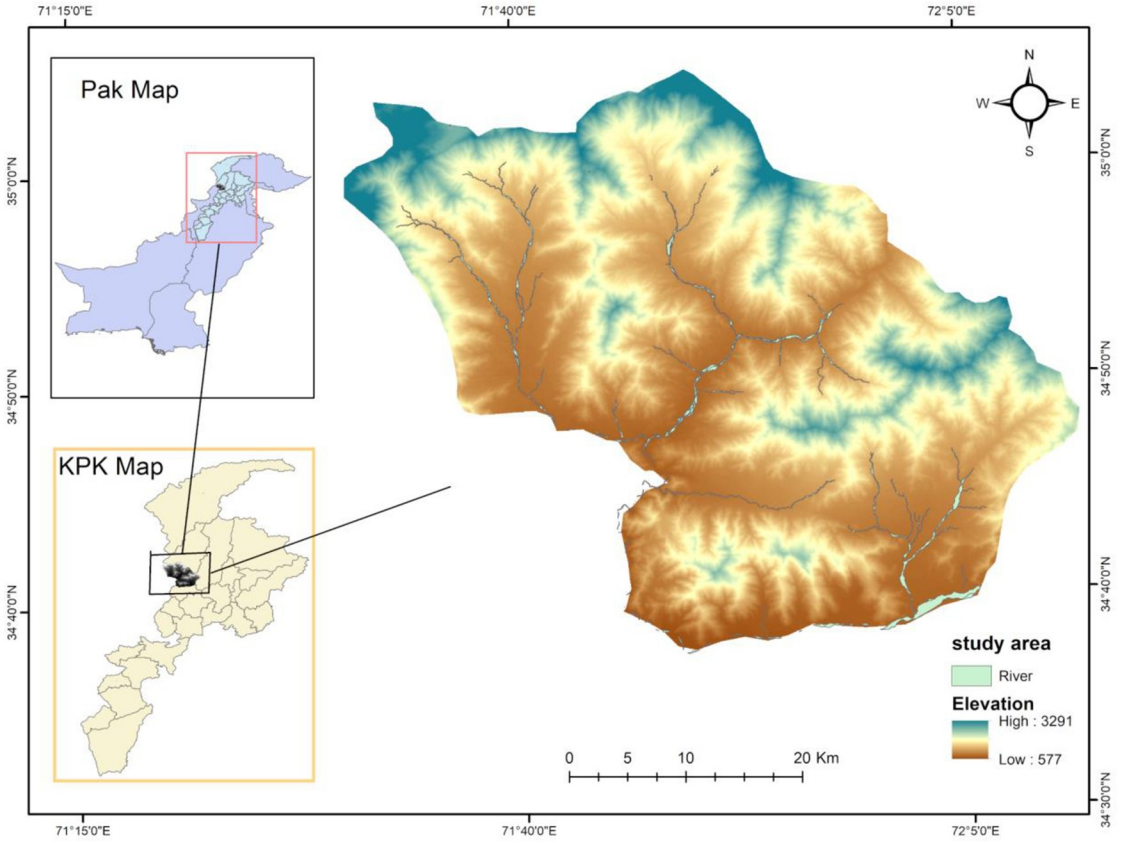


**Fig 1. Study area.**

https://doi.org/10.1371/journal.pone.0229153.g001

susceptibility mapping greatly relies on the accuracy of previous floods events [7,25,49]. In the present study, the flood inventory database was created after identifying 154 flood points using existing flood reports of the National Disaster Management Authority, Pakistan, Provincial Disaster Management Authority, Khyber Pakhtunkhwa, field surveys, and interpretation of satellite and Goggle earth images before and after the 2010 devastating flood in the target area. Based on the literature reviews, 70% of flooded locations (107 locations) were selected randomly as a training dataset to prepare the flood hazard map and 30% of the locations (47 locations) were used for validation of the results (Fig 2) [7,26,50].

## 2.3 Identification of flood triggering and causal factors

To evaluate the flood vulnerability, it was necessary to investigate a series of flood triggering and causal factors and their relationship with flooding [51,52]. In past studies, different flood-controlling factors have been used [1,12,13]. There is no specific guideline for selecting flood-controlling factors that affect flood occurrence. The selection of flood-controlling factors is an important step for flood hazard mapping and depends on physical and natural characteristics of the study area and data availability [18,53]. The methodology adapted for this study is shown in Fig 3. To prepare the flood susceptibility map for the PRB, various satellite images and ancillary datasets were acquired from government organizations and web sources: (i) Advanced Spaceborne Thermal Emission and Reflection Radiometer Digital Elevation Model

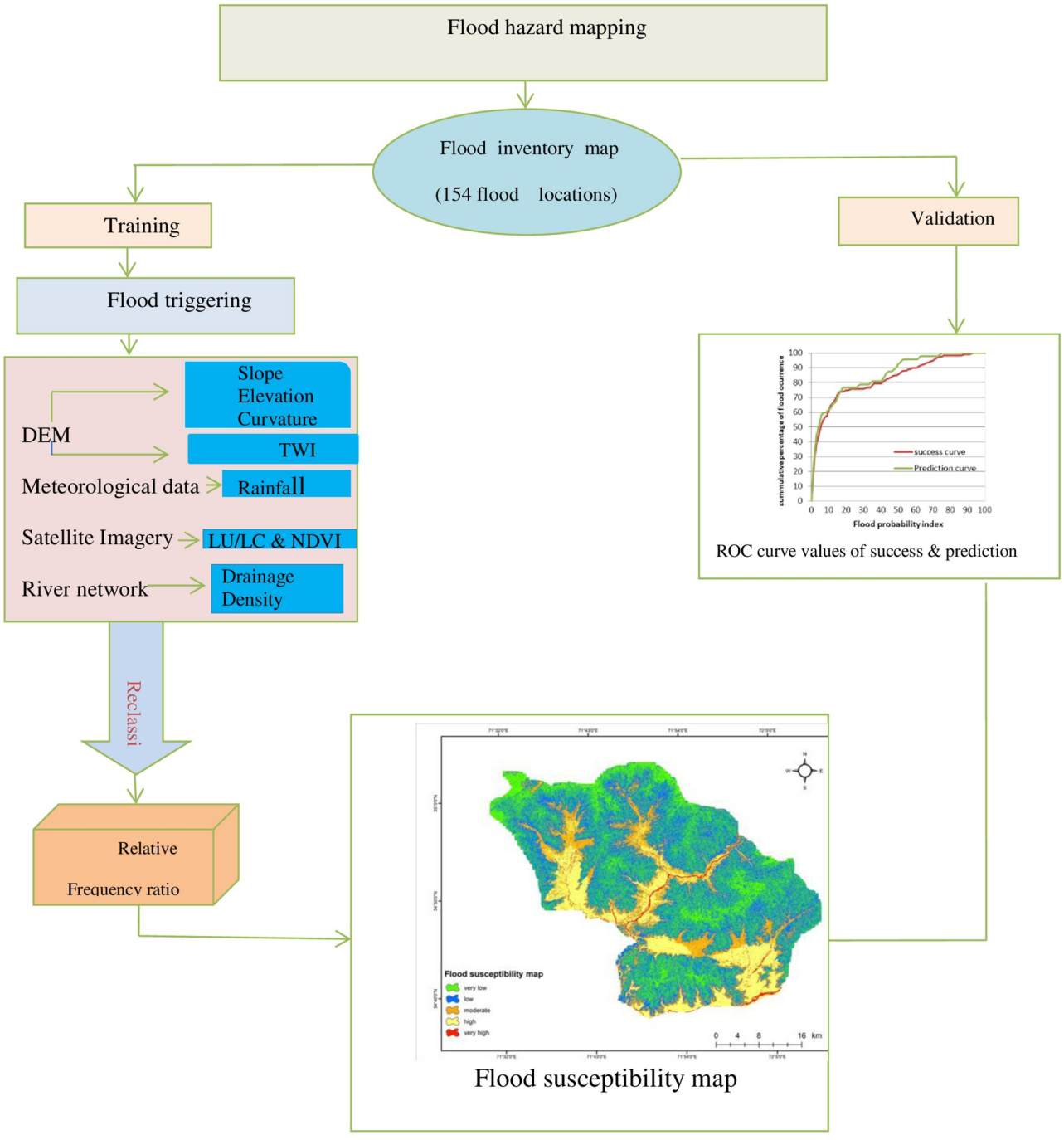


**Fig 2. Historical floods inventory map.**

https://doi.org/10.1371/journal.pone.0229153.g002

(ASTER DEM) of 30 m spatial resolution; (ii) Landsat 8 (OLI) imagery (Date: 19-September-2018) are downloaded from USGS official website (https://earthexplorer.usgs.gov); and (iii) monthly rainfall data from 1980 to 2016 collected from the Regional Meteorological Center, Peshawar. In this study, we have identified and selected eight flood causative factors, namely, slope, elevation, curvature, TWI, land use and land cover (LULC), rainfall, NDVI, and

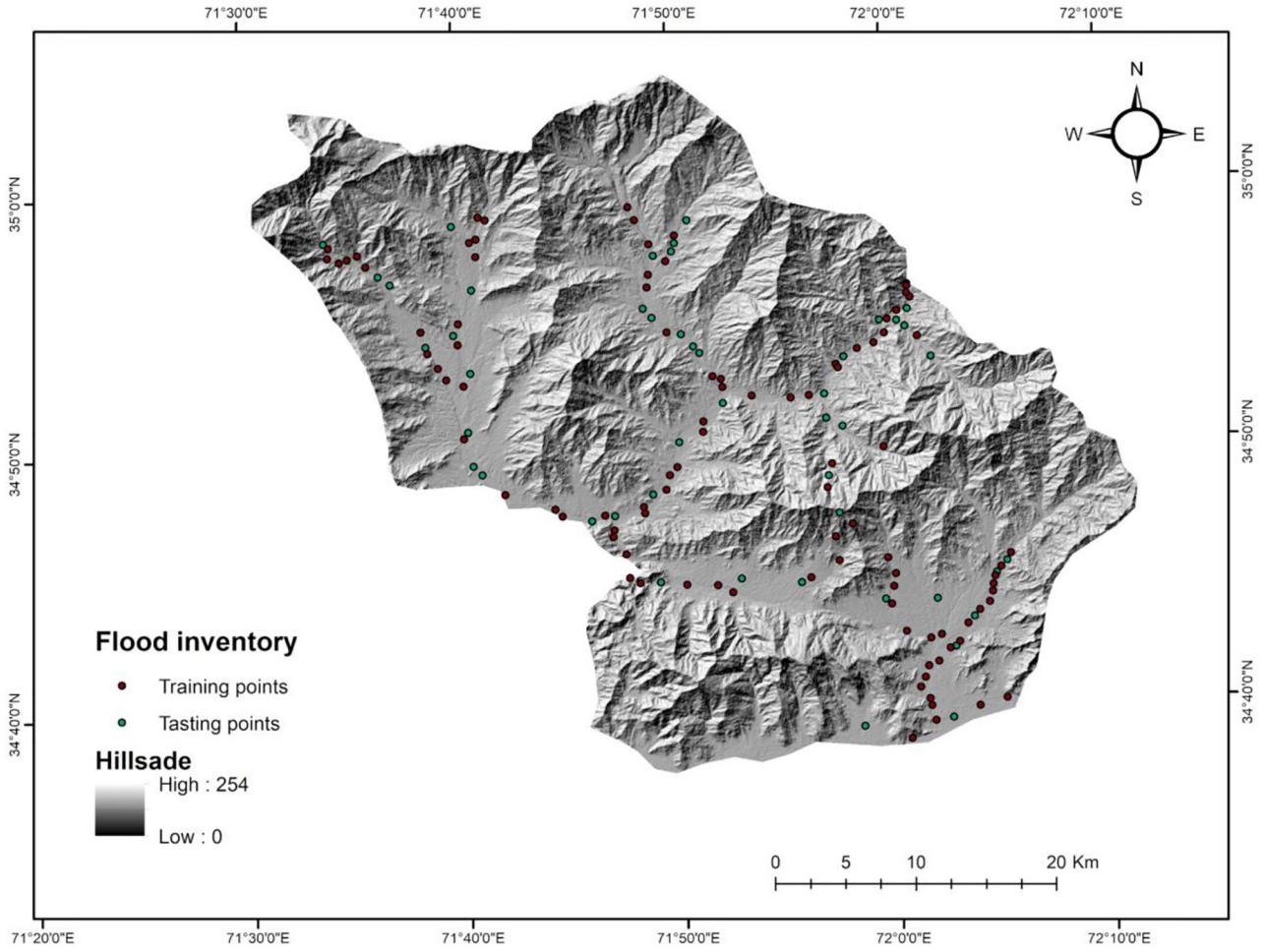


**Fig 3. Flow chart of the methodology adopted for flood hazard mapping in PRB.**

https://doi.org/10.1371/journal.pone.0229153.g003

drainage density to generate thematic layers for flood hazard mapping based on a literature review and local conditions [10,13,20]. Moreover, ArcGIS (10.2), SAGA GIS, and Erdas were used to generate the required thematic layers. The relationship of each factor with flooding is discussed below in Table 1 and illustrated in Figs 4 and 5.

## 2.4 Relative frequency ratio model

Flood hazard assessment is an important technique in hydrological studies. In this study, an RFR model is used to map flood prone zones in the PRB. FR is a bivariate statistical analysis method, based on the spatial distribution (probability) dependent factor (flood location) and flood triggering and causal factors (i.e., slope, elevation, etc.) [25,42].

The bivariate probability of each independent flood triggering factor was determined by its relationship with flood occurrence [1,25]. The higher the bivariate probability (greater than 1) the stronger is the correlation between flood incidence and flood triggering factors, and the lower the probability (less than 1), the weaker the correlation [1,25,50].

**Table 1. Identification of flood triggering and causal factors.**

| Flood triggering and causal factors | Procedure of preparation of each factor and its relationship with flood susceptibility |
|---|---|
| Elevation | • Elevation is one of the prime factors controlling floods in a region [54].<br>• Lower and lowland areas may get flooded faster as water flows from high altitude to low regions. Areas located at a higher elevation usually have a lower probability of flooding compared to lowland areas [12,53].<br>• In this study, the elevation map was prepared from ASTER DEM 30 m resolution and classified into seven classes using the natural break method in ArcGIS 10.2 (Fig 4a). |
| Slope angle | • In hydrological studies, slope plays an important role; it regulates surface water flow [7,12].<br>• Slope controls the surface runoff and the intensity of water flow that provokes erosion of soil and vertical percolation [32].<br>• The area having a lower slope is more exposed to flooding [53].<br>• In the PRB, the angle variation in slope ranges from 0˚–68˚. The slope map was directly created from ASTER DEM using the surface tool in ArcGIS 10.2 (Fig 4b). |
| Drainage density | • Drainage density is defined as the ratio of the total length of the watershed channels to the total area of the basin [26].<br>• Drainage density has a direct relationship with flooding. A higher likelihood of flooding is directly linked to higher drainage density as it indicates a high surface runoff [43].<br>• The stream network was extracted from ASTER DEM and a drainage density map was developed by applying line density in spatial analyst ArcGIS (10.2).<br>• The drainage density map was classified into five classes using a natural break (Fig 4c). |
| Land use/ land cover | • Land use and land cover (LULC) are important factors in generating surface runoff and potential flooding in a watershed [55,56].<br>• LULC directly or indirectly affects penetration, evapotranspiration, and surface runoff generation [1,54].<br>• The LULC map was prepared from the Landsat-8 (OLI) satellite imagery (Fig 4d) through supervised classification techniques using a maximum likelihood algorithm in Erdas 2015.<br>• The LULC map was classified into seven classes: shrubs, agriculture, natural vegetation, water bodies, built area, barren land, and snow cover. |
| Curvature | • Curvature is regarded as one of the flood-conditioning factors in most literature [9,12].<br>• Curvature is the rate of change in slope gradient in a specific direction: the values represent the morphology of the topography [22,25].<br>• A positive curvature means that the slope gradient is convex in the upward direction, a zero value represents no curvature, and a negative value indicates the slope is concave upward [8].<br>• The curvature map was prepared from ASTER DEM in ArcGIS 10.12 (Fig 5a). |
| Normalized Difference Vegetation Index | • The NDVI is another factor that is a valuable index in assessing vegetation coverage and its outcome on flooding in a basin [25].<br>• The NDVI normally ranges from -1 to +1[7].<br>• The NDVI values ranged from -0.15 to 0.53 in the study region.<br>• The NDVI map was prepared from a satellite image of Landsat 8 (OLI). The NDVI values were calculated using equation Eq 1 [7].<br>$$\mathrm{NDVI} = (NIR - VIS)/(NIR + VIS) \quad (1)$$<br>where *VIS* and *NIR* are the spectral reflectance measurement acquired in the visible (red) and near-infrared region respectively (Fig 5b). |
| Topographic wetness index | • TWI is generally used to measure the effect of topography on runoff generation and the amount of flow accumulation at any position in a river catchment [12,25].<br>• TWI was calculated from the flowing formula;<br>$$TWI = \ln[\frac{As}{\tan(\beta)}] \quad (2)$$<br>where *As* is the upstream contributing area and $\beta$ is the slope gradient.<br>• High TWI regions have a high vulnerability to flooding and lower TWI regions have lower flood vulnerability [57].<br>• TWI has been calculated directly by processing ASTER DEM in SAGA GIS (Fig 5c). |
| Rainfall | • In Pakistan, flooding usually occurs after heavy rainfall.<br>• Literature indicates that rainfall has a direct relationship with river discharge and a large amount of rainfall in a short time can generate flash floods in semi-arid regions [12,43,53,54].<br>• The monthly rainfall data from 1980 to 2016 were collected from the Regional Meteorological Center (RMC) Peshawar.<br>• The rainfall distribution map has been prepared from average rainfall through Inverse Distance Weighting (IDW) Interpolation in ArcGIS 10.2 (Fig 5d). |

https://doi.org/10.1371/journal.pone.0229153.t001

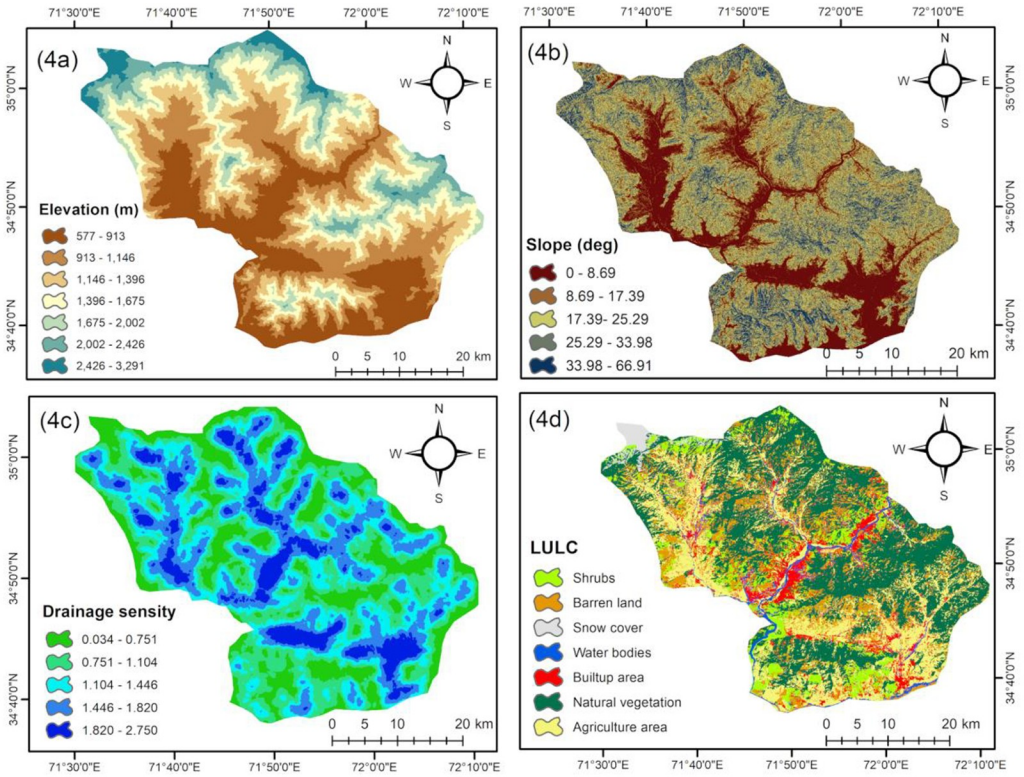


**Fig 4. Flood conditioning factors: (a) elevation, (b) slope, (c) drainage density, (d) LULC.**

https://doi.org/10.1371/journal.pone.0229153.g004

The FR values were calculated using (Eq 3) for all sub-classes of flood triggering factors based on their relationships with flood inventory, as shown in Table 2.

$$\mathrm{FR} = \frac{\text{Flood points in factor class}/\text{Total flood points}}{\text{Factor class area}/\text{Total area}} \tag{3}$$

In the next step, the FR was normalized in a range of probability values [0, 1] as relative frequency (RF) using Eq 4.

$$\mathrm{LRF} = \frac{\text{Factor class FR}}{\sum \text{Factor classes FR}} \tag{4}$$

After the normalization, the RF still has the drawback of considering all causative factors as having equal weight. To overcome this problem and to find the mutual interrelationship among flood causative factors, a predictor rate (PR), or weight, was calculated by rating each flood causative factor with the training data set (Eq 5) [58–60].

$$PR = (RF_{max} - RF_{min})/(RF_{max} - RF_{min})Min \tag{5}$$

Finally, the flood susceptibility index was obtained by the summation of the PR of each factor and the RF of each class using Eq 6.

$$FSI = \sum_{i=1}^{n} PR_i \times RF_i \tag{6}$$

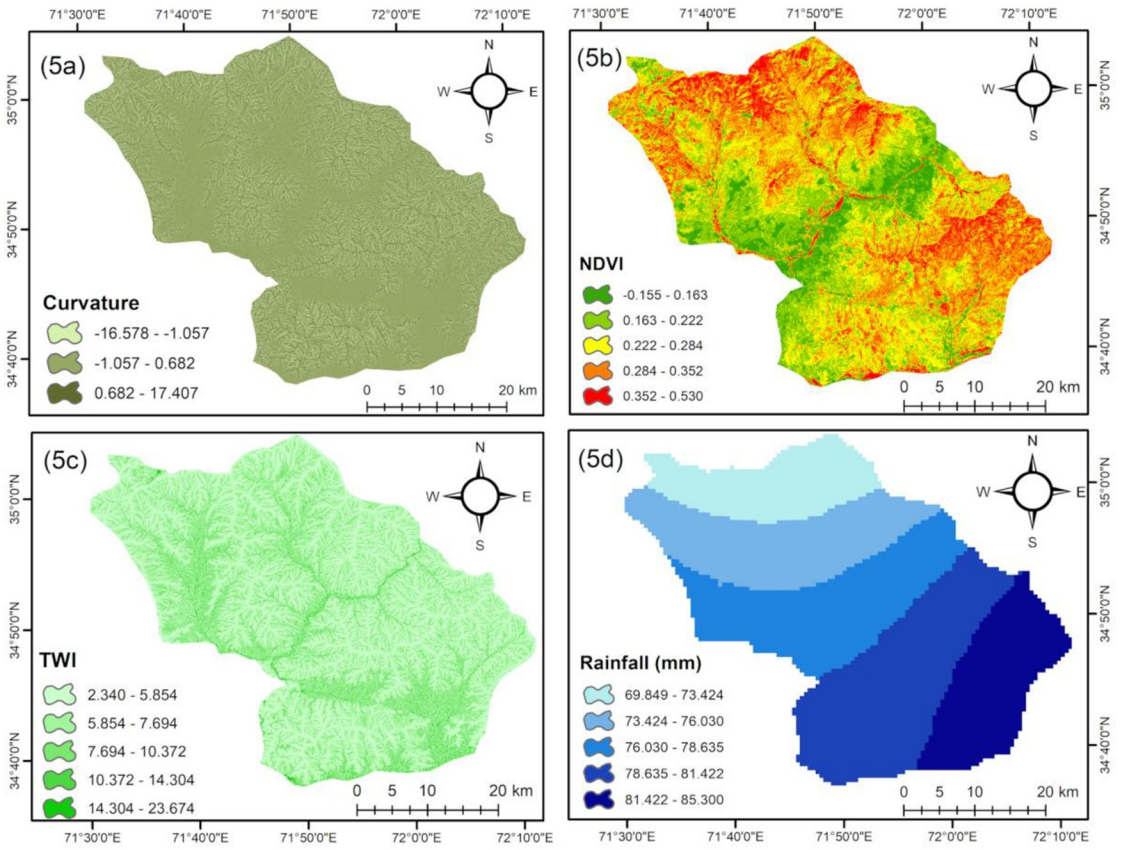


**Fig 5. Flood conditioning factors: (a) curvature, (b) NDVI, (c) TWI, (d) rainfall.**

https://doi.org/10.1371/journal.pone.0229153.g005

where $PR_i$ is the weight of each triggering factor, $RF$ is the class weight of each subclass of flood triggering factor, and $n$ is the number of factors. In this study, $n = 8$.

## 3. Results and discussion

In this study, the flood susceptibility of the PRB has been assessed by using an integrated approach of the bivariate statistical method (FR) with geospatial techniques. FR was used to calculate the correlation between flood occurrence and flood triggering factors. Table 2 shows the relationship between different flood causative factors, sub-classes, and flood occurrence in the PRB. Eight flood-triggering factors, namely, elevation, slope, drainage density, LULC, curvature, NDVI, TWI, and rainfall were used in the study. There is a direct positive relationship between FR and flood probability.

Elevation is an important factor of flood occurrence, as water always flows from higher locations to low land areas [52]. The elevation class 577–913 m has the maximum RF value of 0.56, followed by 913–1146 m and 1146–1675 m with RF values of 0.15 and 0.12, respectively. The analysis reveals that almost 65% of past floods occurred in the first three classes of elevation. Elevations higher than 2436 m have the lowest RF value (0.00, see Table 2). These results are in agreement with previous studies, which found a low probability of flood occurrence at higher elevated regions and a high probability of flooding in lowland areas [54,57].

Slope regulates the incidence of flooding, as lowland areas in the rainy season have a strong connection with the flood state. It has been reported that a lower slope gradient has more

**Table 2. Calculation results of FR and RF for all classes of factors.**

| Factors | Factor classes | No of points | % of points | class area | % of class area | FR | RF |
|---|---|---|---|---|---|---|---|
| Elevation | 1 | 59400 | 61.11 | 425764 | 21.75 | 2.81 | 0.56 |
| | 2 | 16200 | 16.67 | 444873 | 22.72 | 0.73 | 0.15 |
| | 3 | 10800 | 11.11 | 377469 | 19.28 | 0.58 | 0.12 |
| | 4 | 7200 | 7.41 | 299902 | 15.32 | 0.48 | 0.10 |
| | 5 | 2700 | 2.78 | 216801 | 11.07 | 0.25 | 0.05 |
| | 6 | 900 | 0.93 | 139457 | 7.12 | 0.13 | 0.03 |
| | 7 | 0.00 | 0.00 | 53488 | 2.73 | 0.00 | 0.00 |
| Slope | 1 | 68400 | 70.37 | 466272 | 23.82 | 2.95 | 0.68 |
| | 2 | 12600 | 12.96 | 400501 | 20.46 | 0.63 | 0.15 |
| | 3 | 10800 | 11.11 | 477898 | 24.41 | 0.46 | 0.10 |
| | 4 | 4500 | 4.63 | 416184 | 21.26 | 0.22 | 0.05 |
| | 5 | 900 | 0.93 | 196899 | 10.06 | 0.09 | 0.02 |
| Drainage density | 1 | 2700 | 2.78 | 389221 | 19.96 | 0.14 | 0.02 |
| | 2 | 7200 | 7.41 | 511734 | 26.24 | 0.28 | 0.04 |
| | 3 | 18000 | 18.52 | 444233 | 22.78 | 0.81 | 0.12 |
| | 4 | 33300 | 34.26 | 417495 | 21.41 | 1.6 | 0.24 |
| | 5 | 36000 | 37.04 | 187554 | 9.62 | 3.85 | 0.58 |
| LULC | 1 | 900 | 0.01 | 184627 | 0.09 | 0.10 | 0.01 |
| | 2 | 7200 | 0.07 | 232148 | 0.12 | 0.63 | 0.05 |
| | 3 | 0.00 | 0.00 | 28053 | 0.01 | 0.00 | 0.00 |
| | 4 | 23400 | 0.24 | 55824 | 0.03 | 8.45 | 0.64 |
| | 5 | 17100 | 0.18 | 172316 | 0.09 | 2.00 | 0.15 |
| | 6 | 14400 | 0.15 | 872325 | 0.44 | 0.33 | 0.03 |
| | 7 | 34200 | 0.35 | 415251 | 0.21 | 1.66 | 0.13 |
| Curvature | 1 | 81000 | 8.330 | 329225 | 16.82 | 0.50 | 0.23 |
| | 2 | 83700 | 86.11 | 1293895 | 66.09 | 1.30 | 0.61 |
| | 3 | 54000 | 5.560 | 334632 | 17.09 | 0.33 | 0.15 |
| NDVI | 1 | 27000 | 27.78 | 210062 | 10.73 | 2.59 | 0.43 |
| | 2 | 17100 | 17.59 | 450336 | 23.01 | 0.76 | 0.13 |
| | 3 | 18000 | 18.52 | 536189 | 27.39 | 0.68 | 0.11 |
| | 4 | 17100 | 17.59 | 476438 | 24.34 | 0.72 | 0.12 |
| | 5 | 18000 | 18.52 | 284424 | 14.53 | 1.27 | 0.21 |
| TWI | 1 | 19800 | 20.37 | 817198 | 41.74 | 0.49 | 0.04 |
| | 2 | 32400 | 33.33 | 725250 | 37.05 | 0.90 | 0.08 |
| | 3 | 20700 | 21.30 | 299045 | 15.27 | 1.39 | 0.12 |
| | 4 | 18900 | 19.44 | 90685 | 4.63 | 4.20 | 0.37 |
| | 5 | 54000 | 5.560 | 25574 | 1.31 | 4.25 | 0.38 |
| Rainfall | 1 | 9000 | 0.10 | 268834 | 13.78 | 0.76 | 0.14 |
| | 2 | 19800 | 0.21 | 387366 | 19.86 | 1.17 | 0.21 |
| | 3 | 28800 | 0.30 | 450908 | 23.12 | 1.00 | 0.26 |
| | 4 | 14400 | 0.15 | 514166 | 26.37 | 0.64 | 0.11 |
| | 5 | 22500 | 0.24 | 328400 | 16.84 | 1.56 | 0.28 |

https://doi.org/10.1371/journal.pone.0229153.t002

chances of flooding and flood events [51,56]. The infiltration process is also partly controlled by the slope gradient. An increasing gradient decreases the process of infiltration but increases the surface runoff; as a result, in regions having a sudden descent gradient, an enormous extent of water becomes stagnant and causes flood conditions [61]. The results show that the two

lower slope gradient classes, i.e., <6.8˚ and 6.8˚–15.4˚ have the highest RF value of 0.68 and 0.15, respectively. In contrast, the slope gradient above 29.4˚ shows the lowest RF value of 0.02 (Table 2). Approximately 68% of fast floods occurred in PRB areas having slope lower than 25˚. Fig 4b indicated that the lower slope gradients are pointed on both sides of the river.

Drainage density is considered an essential element of flooding. The higher likelihood of flooding is strongly linked to higher drainage density as it points toward a greater surface runoff [54]. In this study, the drainage density has a direct relationship with flooding. The probability of flooding increases with an increase in drainage density and decreases with a decrease in drainage density. Drainage density was divided into five classes using the natural break method (Fig 4c). The class 1.82–2.75 km/km$^2$ and 0.034–0.75 km/km$^2$ have the highest and lowest probability of flooding with RF values of 0.58 and 0.2, respectively (Table 2). High drainage density refers to high surface runoff, therefore, high flood probability exists in areas having high drainage density [43,54].

Land use patterns reveal the type of utilization of land by people and natural processes [7,12]. Urban areas increase runoff due extensive impervious soil and fallow farmland increases runoff where there is no vegetation cover to control and prevent the rapid flow of water to the soil surface. There is risk of flooding and soil erosion in those areas; therefore, they are the most vulnerable areas to flooding. For LULC, the maximum weights were allocated to water bodies (RF = 0.61), followed by built-up areas (0.15) and agriculture areas (0.13), while forest and snow cover are least vulnerable areas in the region with RF values of 0.00 and 0.3, respectively (Table 2). Built-up areas located in proximity to rivers are most vulnerable to flooding due to their economic resources, infrastructure, and large population [7,12,25].

Similarly, curvature is also an important factor and represents the morphology of the topography [12,25,62]. The curvature map is classified into three classes. A positive value of curvature represents a convex surface, zero a flat surface, and a negative value a concave surface [7,54]. The results show that the highest RF was obtained for the flat surface at the rate of 0.61, while the lowest RF was obtained for the concave surface at 0.15 (Table 2). It was observed that approximately 83% past flood had occurred in flat and convex shape slopes.

The NDVI is another important conditioning factor of flooding. The index values range from -1 to +1[7]. Khosravi et al. [25] stated that the negative values show water and the positive values show vegetation so, NDVI has negative relationship with flooding: higher NDVI values indicate lower probability of flood and lower NDVI values indicate higher flood probability. In this study, the NDVI values range from -0.15 to 0.53 and were classified into five classes using a natural break method (Fig 5b). For the class -0.15 to 0.16, the RF was highest 0.43 (Table 2), which means that there is a high probability of flooding in the study region [43].

The TWI was classified into five classes: <5.85, 5.85–7.69, 7.69–10.37, 10.37–14.30, and 14.30–23.67 (Fig 5c). The RF values for the TWI classes of 14.30–23.67 and 10.37–14.30 were calculated as the highest at 0.38 and 0.37, respectively. Similarly, the RF value for the TWI class of <5.85 was lowest at 0.04 (Table 2). TWI has a direct positive relationship with flooding [12,25]. The higher TWI class refers to higher chances of flooding in the watershed [10]. The results indicate that the higher TWI was found in the south, northeast, and middle of the study area (represented with a blue color in Fig 5c), and a low TWI was mostly present in the north and in steep slopes.

Except for glaciers, rainfall is the only source of water in the study region. A sudden rainfall in an area can cause flash flood conditions in semi-arid regions [12]. A large number of previous studies have established a relationship between rainfall and flooding [17,52,54]. The PRB is characterized by semi-arid climatic conditions, where an enormous amount of rainfall occurs summer season due Asian monsoon system which causes flash flood [63]. The rainfall

**Table 3. Classification of different hazard classes.**

| Hazard class | Class area (sq.km) | % of Area |
|---|---|---|
| Very low | 509 | 29 |
| Low | 723 | 42 |
| Medium | 248 | 14 |
| High | 240 | 14 |
| Very high | 21 | 1 |
| Total | 1741 | 100 |

https://doi.org/10.1371/journal.pone.0229153.t003

map was reclassified into five classes with natural breaks. The highest RF value (0.29) was observed for class >81.43 mm followed by class 76.03–78.63, 73.42–76.03, and 69.84–73.42 with RF values of 0.26, 0.21, and 0.14, respectively (Table 2). The lowest RF value of 0.11 was observed for class 78.63–81.42 mm. It is interesting to note that the class 78.63–81.42 mm is the second highest rainfall region but the least vulnerable, because this region is characterized by high elevation, high slope gradient, and dense forest and floods occur in lowland area. Therefore an increase in rainfall has no impact on flooding [25].

After the preparation of all eight layers of flood triggering and causal factors and giving weights to each parameter using FR and RF, a final hazard map was obtained by summation of each factor PR (weight) and each class RF in a raster calculator ArcGIS 10.2 environment using Eq 6. The flood hazard index (FHI) values of the study area are found to lie in the range from 8302 to 100311. The FSI values of the total area were divided in five subclasses using a natural break method: very low, low, medium, high, and very high and indicated in Fig 5. The analysis illustrates that approximately 15% of the total area is in a very high and high flood hazard zone, 14% is in medium, 42% is in low, and 29% is in safe areas (Table 3).

In the study region, the slope has the maximum contribution to flooding with a PR value of 3.98 closely followed by LULC and elevation with PR values of 3.88, 3.41, respectively. The curvature, NDVI, and TWI have a medium influence on flood occurrence with PR values of 2.79, 1.92, and 1.81, respectively, while the drainage density and rainfall are the least important factors with PR values of 1.32 and 1.00, respectively, in determining flood susceptibility in the study region (Table 4). Fig 6 indicated that most of the very high and high risk areas are located near the banks of rivers Panjkora with low slope gradient, low elevation, flat curvature, higher TWI, and higher drainage density. From the final hazard map, it is clear that agriculture practices, commercial activities, or people living in high and very high flood susceptible zones are highly vulnerable to future flooding in the study region.

**Table 4. Calculation results of weights for all conditioning factors.**

| Factor | Min RF | Max RF | (Max-Min) | Min total | PR(weight) |
|---|---|---|---|---|---|
| Elevation | 0 | 0.56 | 0.56 | 0.19 | 3.41 |
| Slope | 0.02 | 0.68 | 0.66 | 0.19 | 3.98 |
| Drainage density | 0.02 | 0.24 | 0.22 | 0.19 | 1.32 |
| Land use | 0 | 0.64 | 0.64 | 0.19 | 3.88 |
| Curvature | 0.15 | 0.61 | 0.46 | 0.19 | 2.79 |
| NDVI | 0.11 | 0.43 | 0.32 | 0.19 | 1.92 |
| TWI | 0.08 | 0.38 | 0.30 | 0.19 | 1.81 |
| Rainfall | 0.11 | 0.28 | 0.17 | 0.19 | 1.00 |

https://doi.org/10.1371/journal.pone.0229153.t004

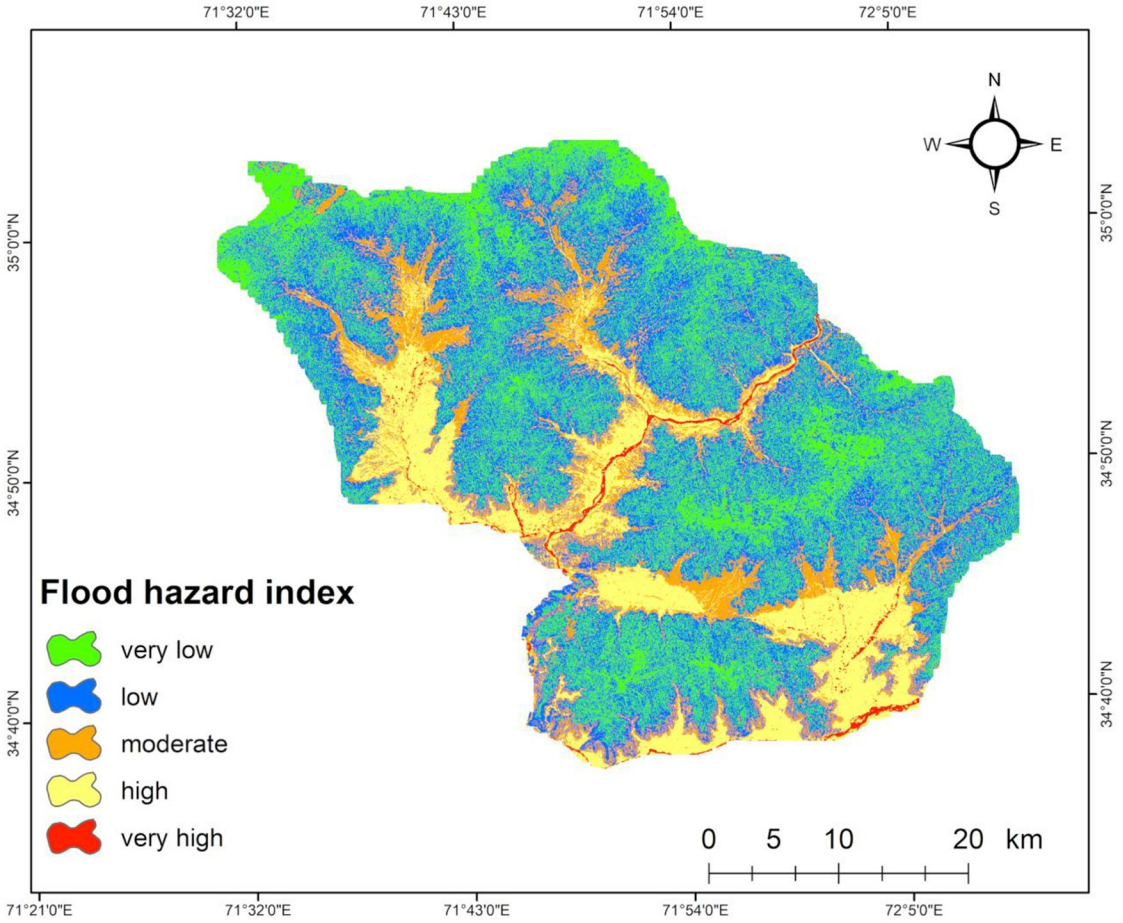


**Fig 6. Flood hazard map of the study area.**

https://doi.org/10.1371/journal.pone.0229153.g006

### 3.1 Validation of flood hazard map

The primary objective of hazard mapping is to demarcate the areas that are prone to flood hazards. There are many models used by researchers to analyze flood susceptibility, but it is essential to validate the results of the model used for flood hazard assessment [61,64]. The receiver operating characteristic (ROC) method is frequently used for the validation of prediction maps [9,53]. Moreover, the method is simple and produces clear and reliable results [25,65]. Many studies have used this method to validate results [1,26]. In this study, we used the ROC method to evaluate the success and prediction rate of the flood hazard map based on the previous flood incidents. To validate the model, we compared the existing flood data with the acquired flood probability map [64,66]. The results of the success rate were obtained using the training data set, and the prediction accuracy was calculated using the validation dataset that was not used in the training process [7,61,67]. The ROC curve for this study is shown in Fig 7, with AUC values of success and prediction accuracy of 82.04% and 84.74%, respectively.

## 4. Conclusion

Flood susceptibility mapping is an important step for future flood management. In hydrological and flood management studies, flood susceptibility maps are widely used to determine flood-prone zones. The present study aimed to assess flood hazards and map the flood-prone

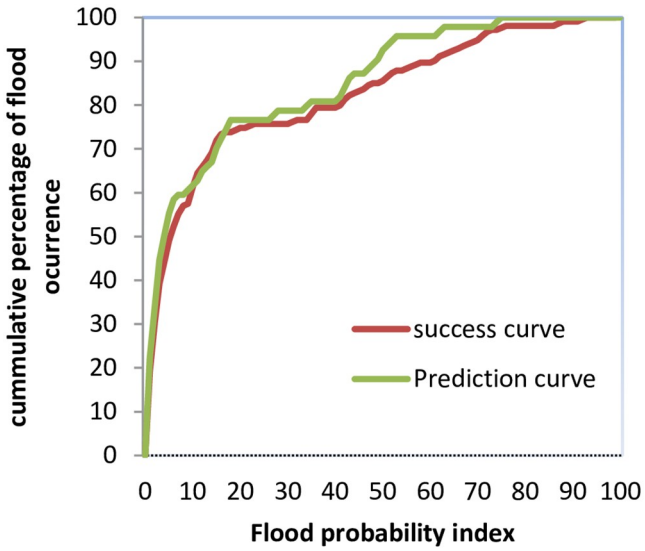


**Fig 7. The ROC curve values of success rate and prediction rate.**

https://doi.org/10.1371/journal.pone.0229153.g007

zones in the PRB, eastern Hindu Kush region. For this purpose, the RFR method was integrated with remote sensing and geospatial techniques to assess and map the flood hazard-prone areas. In this study, we used eight conditioning factors including slope, elevation, TWI, LULC, NDVI, drainage density, curvature, and rainfall to develop flood susceptibility maps. Overall, 154 flood-inundated locations were identified based on the damage and needs assessment report of the 2010 flood, field survey, interpretation of Landsat-7 and google earth images. The flood points were randomly divided into a training data set and testing data set. We used 70% (107 flood locations) of the points for building the model, and the remaining 30% (47 flood locations) points were employed in the validation of the probability model.

The flood hazard area was divided into five subclasses of hazard zones: very high, high, medium, low, and very low. The study found that approximately 15% of the total area is highly prone to flood hazard, 14% is moderately susceptible, 42% is low, and approximately 29% is very low. Furthermore, the study indicates that the high flood-prone areas are situated in the mid, southern, and western portions of the study area, as these areas are near the river with a low slope gradient, flat curvature, low elevation, high TWI value, and high drainage density. The ROC curve was used to measure the efficiency of the model and evaluate the results. The validation results showed good prediction efficiency with AUC values of success rate at 82.04% and of prediction rate at 84.74% of the flood susceptibility map. Therefore, the flood susceptibility map generated in this study can be considered an important tool to incorporate in flood risk management plans for disaster managers, decision-makers, and engineers. Based on the findings of this study, the concerned authorities can adopt appropriate mitigation and preparedness measures to minimize the impacts of prevailing and future floods.

## Supporting information

**S1 Data.**
(XLSX)

**S2 Data.**
(XLSX)

**S3 Data.**
(XLSX)

**S1 File.**
(RAR)

## Acknowledgments

We would like to thank Regional Meteorological Center, Peshawar for providing us rainfall data and United States Geological survey (USGS) for Landsat- 8 and ASTER DEM images. The authors greatly appreciate the reviewers and editors for their critical comments that greatly helped in improving the quality of this manuscript.

## Author Contributions

**Conceptualization:** Jiquan Zhang.

**Formal analysis:** Kashif Ullah.

**Software:** Kashif Ullah.

**Supervision:** Jiquan Zhang.

**Writing – original draft:** Kashif Ullah.

**Writing – review & editing:** Kashif Ullah, Jiquan Zhang.

## References

1. Samanta RK, Bhunia GS, Shit PK, Pourghasemi HR. Flood susceptibility mapping using geospatial frequency ratio technique: a case study of Subarnarekha River Basin, India. Model Earth Syst Environ. 2018; 4: 395–408. https://doi.org/10.1007/s40808-018-0427-z
2. Zou Q, Zhou J, Zhou C, Song L, Guo J. Comprehensive flood risk assessment based on set pair analysis-variable fuzzy sets model and fuzzy AHP. Stoch Environ Res Risk Assess. 2013; 27: 525–546. https://doi.org/10.1007/s00477-012-0598-5
3. Calil J, Beck MW, Gleason M, Merrifield M, Klausmeyer K, Newkirk S. Aligning natural resource conservation and flood hazard mitigation in California. PLoS One. 2015; 10: 1–14. https://doi.org/10.1371/journal.pone.0132651 PMID: 26200353
4. Gain AK, Mojtahed V, Biscaro C, Balbi S, Giupponi C. An integrated approach of flood risk assessment in the eastern part of Dhaka City. Nat Hazards. 2015; 79: 1499–1530. https://doi.org/10.1007/s11069-015-1911-7
5. Nageswara Rao G. Occurrence of heavy rainfall around the confluence line in monsoon disturbances and its importance in causing floods. Proc Indian Acad Sci Earth Planet Sci. 2001; 110: 87–94. https://doi.org/10.1007/bf02702232
6. Scheuer S, Haase D, Volk M. Integrative assessment of climate change for fast-growing urban areas: Measurement and recommendations for future research. PLoS One. 2017; 12: 1–27. https://doi.org/10.1371/journal.pone.0189451 PMID: 29232695
7. Khosravi K, Pourghasemi HR, Chapi K, Bahri M. Flash flood susceptibility analysis and its mapping using different bivariate models in Iran: a comparison between Shannon's entropy, statistical index, and weighting factor models. Environ Monit Assess. 2016; 188. https://doi.org/10.1007/s10661-016-5665-9 PMID: 27826821
8. Charlton R, Fealy R, Moore S, Sweeney J, Murphy C. Assessing the impact of climate change on water supply and flood hazard in Ireland using statistical downscaling and hydrological modelling techniques. Clim Change. 2006; 74: 475–491. https://doi.org/10.1007/s10584-006-0472-x
9. Tehrany MS, Pradhan B, Jebur MN. Spatial prediction of flood susceptible areas using rule based decision tree (DT) and a novel ensemble bivariate and multivariate statistical models in GIS. J Hydrol. 2013; 504: 69–79. https://doi.org/10.1016/j.jhydrol.2013.09.034

10. Tehrany MS, Pradhan B, Mansor S, Ahmad N. Flood susceptibility assessment using GIS-based support vector machine model with different kernel types. Catena. 2015; 125: 91–101. https://doi.org/10.1016/j.catena.2014.10.017

11. Dandapat K, Panda GK. Flood vulnerability analysis and risk assessment using analytical hierarchy process. Model Earth Syst Environ. 2017; 3: 1627–1646. https://doi.org/10.1007/s40808-017-0388-7

12. Das S. Geographic information system and AHP-based flood hazard zonation of Vaitarna basin, Maharashtra, India. Arab J Geosci. 2018; 11. https://doi.org/10.1007/s12517-018-3933-4

13. Dou X, Song J, Wang L, Tang B, Xu S, Kong F, et al. Flood risk assessment and mapping based on a modified multi-parameter flood hazard index model in the Guanzhong Urban Area, China. Stoch Environ Res Risk Assess. 2018; 32: 1131–1146. https://doi.org/10.1007/s00477-017-1429-5

14. Guo E, Zhang J, Ren X, Zhang Q, Sun Z. Integrated risk assessment of flood disaster based on improved set pair analysis and the variable fuzzy set theory in central Liaoning Province, China. Nat Hazards. 2014; 74: 947–965. https://doi.org/10.1007/s11069-014-1238-9

15. Naulin JP, Payrastre O, Gaume E. Spatially distributed flood forecasting in flash flood prone areas: Application to road network supervision in Southern France. J Hydrol. 2013; 486: 88–99. https://doi.org/10.1016/j.jhydrol.2013.01.044

16. Zhang J, Chen Y. Risk assessment of flood disaster induced by typhoon rainstorms in Guangdong province, China. Sustain. 2019; 11. https://doi.org/10.3390/su11102738

17. Hong H, Panahi M, Shirzadi A, Ma T, Liu J, Zhu AX, et al. Flood susceptibility assessment in Hengfeng area coupling adaptive neuro-fuzzy inference system with genetic algorithm and differential evolution. Sci Total Environ. 2018; 621: 1124–1141. https://doi.org/10.1016/j.scitotenv.2017.10.114 PMID: 29074239

18. Kia MB, Pirasteh S, Pradhan B, Mahmud AR, Sulaiman WNA, Moradi A. An artificial neural network model for flood simulation using GIS: Johor River Basin, Malaysia. Environ Earth Sci. 2012; 67: 251–264. https://doi.org/10.1007/s12665-011-1504-z

19. Vojtek M, Vojteková J. Flood susceptibility mapping on a national scale in Slovakia using the analytical hierarchy process. Water (Switzerland). 2019; 11. https://doi.org/10.3390/w11020364

20. Abbaszadeh P. Improving Hydrological Process Modeling Using Optimized Threshold-Based Wavelet De-Noising Technique. Water Resour Manag. 2016; 30: 1701–1721. https://doi.org/10.1007/s11269-016-1246-5

21. Danandeh A, Kahya E. A Pareto-optimal moving average multigene genetic programming model for daily streamflow prediction A Pareto-optimal moving average multigene genetic programming model for daily streamflow prediction. 2017. https://doi.org/10.1016/j.jhydrol.2017.04.045

22. Wang Z, Lai C, Chen X, Yang B, Zhao S, Bai X. Flood hazard risk assessment model based on random forest. J Hydrol. 2015; 527: 1130–1141. https://doi.org/10.1016/j.jhydrol.2015.06.008

23. Mukerji A, Chatterjee C, Singh Raghuwanshi N. Flood forecasting using ANN, neuro-fuzzy, and neuro-GA models. J Hydrol Eng. 2009; 14: 647–652. https://doi.org/10.1061/(ASCE)HE.1943-5584.0000040

24. Nandi A, Mandal A, Wilson M, Smith D. Flood hazard mapping in Jamaica using principal component analysis and logistic regression. Environ Earth Sci. 2016; 75: 1–16. https://doi.org/10.1007/s12665-016-5323-0

25. Khosravi K, Nohani E, Maroufinia E, Pourghasemi HR. A GIS-based flood susceptibility assessment and its mapping in Iran: a comparison between frequency ratio and weights-of-evidence bivariate statistical models with multi-criteria decision-making technique. Nat Hazards. 2016; 83: 947–987. https://doi.org/10.1007/s11069-016-2357-2

26. Rahmati O, Pourghasemi HR, Zeinivand H. Flood susceptibility mapping using frequency ratio and weights-of-evidence models in the Golastan Province, Iran. Geocarto Int. 2016; 31: 42–70. https://doi.org/10.1080/10106049.2015.1041559

27. Dano UL, Balogun AL, Matori AN, Yusouf KW, Abubakar IR, Mohamed MAS, et al. Flood susceptibility mapping using GIS-based analytic network process: A case study of Perlis, Malaysia. Water (Switzerland). 2019; 11. https://doi.org/10.3390/w11030615

28. Cao C, Xu P, Wang Y, Chen J, Zheng L, Niu C. Flash flood hazard susceptibility mapping using frequency ratio and statistical index methods in coalmine subsidence areas. Sustain. 2016; 8. https://doi.org/10.3390/su8090948

29. Haghizadeh A, Siahkamari S, Haghiabi AH, Rahmati O. Forecasting flood-prone areas using Shannon's entropy model. J Earth Syst Sci. 2017; 126. https://doi.org/10.1007/s12040-017-0819-x

30. Couasnon A, Sebastian A, Morales-Nápoles O. A Copula-based bayesian network for modeling compound flood hazard from riverine and coastal interactions at the catchment scale: An application to the houston ship channel, Texas. Water (Switzerland). 2018; 10. https://doi.org/10.3390/w10091190

31. Siahkamari S, Haghizadeh A, Zeinivand H, Tahmasebipour N, Rahmati O. Spatial prediction of flood-susceptible areas using frequency ratio and maximum entropy models. Geocarto Int. 2018; 33: 927–941. https://doi.org/10.1080/10106049.2017.1316780

32. Jahangir MH, Mousavi Reineh SM, Abolghasemi M. Spatial predication of flood zonation mapping in Kan River Basin, Iran, using artificial neural network algorithm. Weather Clim Extrem. 2019; 25: 100215. https://doi.org/10.1016/j.wace.2019.100215

33. Tiwari MK, Chatterjee C. Uncertainty assessment and ensemble flood forecasting using bootstrap based artificial neural networks (BANNs). J Hydrol. 2010; 382: 20–33. https://doi.org/10.1016/j.jhydrol.2009.12.013

34. Chen W, Pourghasemi HR, Panahi M, Kornejady A, Wang J, Xie X, et al. Spatial prediction of landslide susceptibility using an adaptive neuro-fuzzy inference system combined with frequency ratio, generalized additive model, and support vector machine techniques. Geomorphology. 2017; 297: 69–85. https://doi.org/10.1016/j.geomorph.2017.09.007

35. Ozdemir A, Altural T. A comparative study of frequency ratio, weights of evidence and logistic regression methods for landslide susceptibility mapping: Sultan mountains, SW Turkey. J Asian Earth Sci. 2013; 64: 180–197. https://doi.org/10.1016/j.jseaes.2012.12.014

36. Youssef AM, Pradhan B, Sefry SA. Flash flood susceptibility assessment in Jeddah city (Kingdom of Saudi Arabia) using bivariate and multivariate statistical models. Environ Earth Sci. 2016; 75: 1–16. https://doi.org/10.1007/s12665-015-4830-8

37. Nicu IC. Frequency ratio and GIS-based evaluation of landslide susceptibility applied to cultural heritage assessment. J Cult Herit. 2017; 28: 172–176. https://doi.org/10.1016/j.culher.2017.06.002

38. Regmi AD, Yoshida K, Pourghasemi HR, DhitaL MR, Pradhan B. Landslide susceptibility mapping along Bhalubang—Shiwapur area of mid-Western Nepal using frequency ratio and conditional probability models. J Mt Sci. 2014; 11: 1266–1285. https://doi.org/10.1007/s11629-013-2847-6

39. Arabameri A, Rezaei K, Pourghasemi HR, Lee S, Yamani M. GIS-based gully erosion susceptibility mapping: a comparison among three data-driven models and AHP knowledge-based technique. Environ Earth Sci. 2018; 77: 0. https://doi.org/10.1007/s12665-018-7808-5

40. Aditian A, Kubota T, Shinohara Y. Comparison of GIS-based landslide susceptibility models using frequency ratio, logistic regression, and artificial neural network in a tertiary region of Ambon, Indonesia. Geomorphology. 2018; 318: 101–111. https://doi.org/10.1016/j.geomorph.2018.06.006

41. Shahabi H, Ahmad BB, Khezri S. Evaluation and comparison of bivariate and multivariate statistical methods for landslide susceptibility mapping (case study: Zab basin). Arab J Geosci. 2013; 6: 3885–3907. https://doi.org/10.1007/s12517-012-0650-2

42. Shafapour M, Jebur MN, Honghttps H, Chenhttps W. GIS-based spatial prediction of flood prone areas using standalone frequency ratio, logistic regression, weight of evidence and their ensemble techniques. 2017; 5705. https://doi.org/10.1080/19475705.2017.1362038

43. Paul GC, Saha S, Hembram TK. Application of the GIS-Based Probabilistic Models for Mapping the Flood Susceptibility in Bansloi Sub-basin of Ganga-Bhagirathi River and Their Comparison. Remote Sens Earth Syst Sci. 2019; 2: 120–146. https://doi.org/10.1007/s41976-019-00018-6

44. Ullah S, You Q, Ullah W, Ali A. Observed changes in precipitation in China-Pakistan economic corridor during 1980–2016. Atmos Res. 2018; 210: 1–14. https://doi.org/10.1016/j.atmosres.2018.04.007

45. Ullah S. Observed changes in temperature extremes over China–Pakistan Economic Corridor during 1980–2016. 2019; 1457–1475. https://doi.org/10.1002/joc.5894

46. Mahmood S, Khan A ul H, Ullah S. Assessment of 2010 flash flood causes and associated damages in Dir Valley, Khyber Pakhtunkhwa Pakistan. Int J Disaster Risk Reduct. 2016; 16: 215–223. https://doi.org/10.1016/j.ijdrr.2016.02.009

47. Mahmood S, Rahman A ur. Flash flood susceptibility modeling using geo-morphometric and hydrological approaches in Panjkora Basin, Eastern Hindu Kush, Pakistan. Environ Earth Sci. 2019; 78: 0. https://doi.org/10.1007/s12665-018-8041-y

48. Rahman A, Mahmood S, Dawood M, Rahman G, Chen F, Rahman A, et al. Impact of Climate Change on Flood Factors and Extent of Damages in the Hindu Kush Region. Oxford Research Encyclopedia of Natural Hazard Science. 2019. https://doi.org/10.1093/acrefore/9780199389407.013.316

49. Merz B, Aerts J, Arnbjerg-Nielsen K, Baldi M, Becker A, Bichet A, et al. Floods and climate: Emerging perspectives for flood risk assessment and management. Nat Hazards Earth Syst Sci. 2014; 14: 1921–1942. https://doi.org/10.5194/nhess-14-1921-2014

50. Aghdam IN, Varzandeh MHM, Pradhan B. Landslide susceptibility mapping using an ensemble statistical index (Wi) and adaptive neuro-fuzzy inference system (ANFIS) model at Alborz Mountains (Iran). Environ Earth Sci. 2016; 75: 1–20. https://doi.org/10.1007/s12665-015-5233-6

51. Radmehr A, Araghinejad S. Flood Vulnerability Analysis by Fuzzy Spatial Multi Criteria Decision Making. Water Resour Manag. 2015; 29: 4427–4445. https://doi.org/10.1007/s11269-015-1068-x

52. Sahana M, Patel PP. A comparison of frequency ratio and fuzzy logic models for flood susceptibility assessment of the lower Kosi River Basin in India. Environ Earth Sci. 2019; 78: 1–27. https://doi.org/10.1007/s12665-019-8285-1

53. Liuzzo L, Sammartano V, Freni G. Comparison between Different Distributed Methods for Flood Susceptibility Mapping. Water Resour Manag. 2019; 33: 3155–3173. https://doi.org/10.1007/s11269-019-02293-w

54. Das S. Geospatial mapping of flood susceptibility and hydro-geomorphic response to the floods in Ulhas basin, India. Remote Sens Appl Soc Environ. 2019; 14: 60–74. https://doi.org/10.1016/j.rsase.2019.02.006

55. Areu-Rangel OS, Cea L, Bonasia R, Espinosa-Echavarria VJ. Impact of urban growth and changes in land use on river flood hazard in Villahermosa, Tabasco (Mexico). Water (Switzerland). 2019; 11: 1–15. https://doi.org/10.3390/w11020304

56. Khosravi K, Pham BT, Chapi K, Shirzadi A, Shahabi H, Revhaug I, et al. A comparative assessment of decision trees algorithms for flash flood susceptibility modeling at Haraz watershed, northern Iran. Sci Total Environ. 2018; 627: 744–755. https://doi.org/10.1016/j.scitotenv.2018.01.266 PMID: 29426199

57. Khosravi K, Melesse AM, Shahabi H, Shirzadi A, Chapi K, Hong H. Flood susceptibility mapping at Ningdu catchment, China using bivariate and data mining techniques. Extrem Hydrol Clim Var. 2019; 419–434.

58. Althuwaynee OF, Pradhan B, Park HJ, Lee JH. A novel ensemble bivariate statistical evidential belief function with knowledge-based analytical hierarchy process and multivariate statistical logistic regression for landslide susceptibility mapping. Catena. 2014; 114: 21–36. https://doi.org/10.1016/j.catena.2013.10.011

59. Acharya TD, Lee DH. Landslide Susceptibility Mapping using Relative Frequency and Predictor Rate along Araniko Highway. KSCE J Civ Eng. 2019; 23: 763–776. https://doi.org/10.1007/s12205-018-0156-x

60. Sangeeta Maheshwari BK. Earthquake-Induced Landslide Hazard Assessment of Chamoli District, Uttarakhand Using Relative Frequency Ratio Method. Indian Geotech J. 2019; 49: 108–123. https://doi.org/10.1007/s40098-018-0334-2

61. Shafizadeh-Moghadam H, Valavi R, Shahabi H, Chapi K, Shirzadi A. Novel forecasting approaches using combination of machine learning and statistical models for flood susceptibility mapping. J Environ Manage. 2018; 217: 1–11. https://doi.org/10.1016/j.jenvman.2018.03.089 PMID: 29579536

62. Razandi Y, Pourghasemi HR, Neisani NS, Rahmati O. Application of analytical hierarchy process, frequency ratio, and certainty factor models for groundwater potential mapping using GIS. Earth Sci Informatics. 2015; 8: 867–883. https://doi.org/10.1007/s12145-015-0220-8

63. Ullah S, You Q, Ullah W, Fiifi D, Hagan T, Ali A, et al. Daytime and nighttime heat wave characteristics based on multiple indices over the China–Pakistan economic corridor. Clim Dyn. 2019; 53: 6329–6349. https://doi.org/10.1007/s00382-019-04934-7

64. Chung CJF, Fabbri AG. Validation of spatial prediction models for landslide hazard mapping. Nat Hazards. 2003; 30: 451–472. https://doi.org/10.1023/B:NHAZ.0000007172.62651.2b

65. Pradhan B, Lee S, Buchroithner MF. A GIS-based back-propagation neural network model and its cross-application and validation for landslide susceptibility analyses. Comput Environ Urban Syst. 2010; 34: 216–235. https://doi.org/10.1016/j.compenvurbsys.2009.12.004

66. Janizadeh S, Avand M, Jaafari A, Van Phong T, Bayat M, Ahmadisharaf E, et al. Prediction success of machine learning methods for flash flood susceptibility mapping in the Tafresh watershed, Iran. Sustain. 2019; 11. https://doi.org/10.3390/su11195426

67. Dou J, Yunus AP, Bui DT, Merghadi A, Sahana M, Zhu Z, et al. Improved landslide assessment using support vector machine with bagging, boosting, and stacking ensemble machine learning framework in a mountainous watershed, Japan. Landslides. 2019. https://doi.org/10.1007/s10346-019-01286-5